

Spatio-temporal point process modelling of fires in Sicily exploring human and environmental factors

Nicoletta D'Angelo^{1*}, Alessandro Albano^{1,2}, Andrea Gilardi³,
Giada Adelfio¹

¹Department of Economics, Business and Statistics, University of Palermo, Palermo, Italy.

²Sustainable Mobility Center (Centro Nazionale per la Mobilità Sostenibile—CNMS).

³MOX - Department of Mathematics, Politecnico di Milano, Milano, Italy.

*Corresponding author(s). E-mail(s): nicoletta.dangelo@unipa.it;
Contributing authors: alessandro.albano@unipa.it;
andrea.gilardi@polimi.it; giada.adelfio@unipa.it;

Abstract

In 2023, Sicily faced an escalating issue of uncontrolled fires, necessitating a thorough investigation into their spatio-temporal dynamics. Our study addresses this concern through point process theory. Each wildfire is treated as a unique point in both space and time, allowing us to assess the influence of environmental and anthropogenic factors by fitting a spatio-temporal separable Poisson point process model, with a particular focus on the role of land usage. First, a spatial log-linear Poisson model is applied to investigate the influence of land use types on wildfire distribution, controlling for other environmental covariates. The results highlight the significant effect of human activities, altitude, and slope on spatial fire occurrence. Then, a Generalized Additive Model with Poisson-distributed response further explores the temporal dynamics of wildfire occurrences, confirming their dependence on various environmental variables, including the maximum daily temperature, wind speed, surface pressure, and total precipitation.

Keywords: Fires, Land usage, Point processes, Spatial analysis, Intensity estimation.

1 Introduction

In recent years, Sicily has experienced an alarming increase in uncontrolled wildfires, establishing it as the Italian region with the highest frequency of fire events and, consequently, the largest burned area. The occurrence of these fires is primarily associated with ignition sources, forest fuels, and environmental conditions (Ganteaume et al., 2013; Hantson et al., 2015; Ricotta and Di Vito, 2014). Ignition sources are typically categorized into natural causes, such as lightning and geological factors, and human causes, both accidental and intentional (Aldersley et al., 2011; Rodrigues and De la Riva, 2014). Human-driven factors, particularly arson (but also, unintentional wildfires), often ignited for purposes like creating new pasture resources or burning stubble, stand out as the primary contributors to wildfires in Sicily, especially in areas where vegetation interfaces with urban structures (Ferrara et al., 2019).

Wildfires pose a significant threat to ecosystems, human settlements, and economic activities, demanding a comprehensive understanding of their spatio-temporal dynamics for effective mitigation and management. The island of Sicily, nestled in the heart of the Mediterranean Sea, has a rich history and diverse landscapes, making it vulnerable to the escalating impacts of climate change, including an increased frequency and intensity of wildfires. In the year 2023, Sicily faced a pronounced wildfire season, underscoring the urgent need for advanced analytical methodologies to unravel the underlying patterns and drivers of these destructive events.

Traditional approaches to wildfire analysis often rely on descriptive statistics and basic spatial visualization, providing limited insights into the effect of environmental, climatic, and anthropogenic factors that contribute to wildfire occurrences. This paper advocates for the application of point process methodology to explore the spatial and temporal dynamics of Sicilian wildfires in 2023.

Point process methodology, rooted in statistical theory, enables the modeling of events occurring in space and time, making it an ideal tool for in-depth analysis of wildfire patterns. By treating each wildfire occurrence as a point in a spatial and temporal domain, we aim to discern potential predictors that may contribute to the ignition of wildfires across the Sicilian landscape.

Moreover, traditional analyses often fall short of capturing the relationships between environmental, climatic, and anthropogenic factors that contribute to wildfires. By exploiting spatio-temporal models, we aim to assess which variables influence the probability of fire occurrence. Including covariates such as land usage, altitude, slope, temperature, precipitation, surface pressure, and wind speed provides a comprehensive framework to understand the underlying mechanisms influencing wildfire patterns.

As noted by Butsic et al. (2015), fires and land usage are intrinsically connected, but research investigating this dynamic is limited. Specifically, the influence of land use on fire ignition is a well-documented phenomenon. Previous papers have shown that land use, particularly the presence of roads, can significantly impact the ignition of fires (Ricotta et al., 2018), with the influence of roads being much stronger in less dense land cover areas. As human activities increasingly encroach upon natural landscapes, understanding the impact of land usage becomes crucial for effective wildfire management. Through the proposed modelling, we seek to quantify the relationship

between different land use types and the probability of fire occurrence, finding areas where human activities may be making the Sicilian landscape worse.

The proposed spatio-temporal separable Poisson point process model seeks to determine the specific contributions of land usage categories on fire occurrences while controlling for other environmental covariates. As a matter of fact, understanding the influence of land usage on wildfire probability is crucial for designing targeted interventions, land-use planning, and developing resilient ecosystems in the face of evolving environmental challenges. We first fit a spatial log-linear Poisson model in order to investigate the influence of land use types on wildfire occurrence, controlling for other environmental covariates. The results highlight the significant effect of human activities, altitude, and slope on spatial fire occurrence. Secondly, a Generalized Additive Model with Poisson-distributed response is fitted to model the temporal fire occurrences, confirming their dependence on various environmental variables, including the maximum daily temperature, wind speed, surface pressure, and total precipitation. This study seeks to contribute not only to the scientific understanding of wildfire dynamics but also to the practical tools necessary for mitigating their impacts on communities and ecosystems.

All the analyses are carried out through the R statistical software (R Core Team, 2024), making particular use of the packages `stopp` (D'Angelo and Adelfio, 2023), `sf` (Pebesma, 2018), and `stars` (Pebesma and Bivand, 2023).

The structure of the paper is as follows. Section 2 presents the data. Section 3 provides an overview of spatio-temporal point processes and the model employed in the paper, while Section 4 illustrates the actual model fitting through the spatial and temporal intensity estimation. Section 5 is devoted to the discussion and conclusions.

2 Data

This section focuses on the description of the data employed in the paper, namely the fire data, which will represent our spatio-temporal point pattern under analysis, and some spatial and/or temporal variables which will serve as covariates, assumed to influence the overall occurrence of points, as typical in point process analysis.

2.1 Fires point pattern

To conduct our analysis, we rely on data obtained from the Fire Information for Resource Management System (FIRMS) platform, accessible for download at the following URL: <https://firms.modaps.eosdis.nasa.gov/download/>. This source provides near real-time active fire locations to natural resource managers.

The variables considered in our study are:

- **Latitude:** Center of 1 km fire pixel, but not necessarily the actual location of the fire as one or more fires can be detected within the 1 km pixel.
- **Longitude:** Center of 1 km fire pixel, but not necessarily the actual location of the fire as one or more fires can be detected within the 1 km pixel.
- **Acq_Date** (Acquisition Date): Date of MODIS acquisition.
- **Acq_Time** (Acquisition Time): Time of acquisition/overpass of the satellite (in UTC).

In particular, `Longitude` and `Latitude` will be used as spatial coordinates of our point pattern, while `Acq_Date` and `Acq_Time` will be combined in a unique variable serving as the time occurrence of the fire, with the smallest detail as the hour of occurrence within a day.

Focusing exclusively on the spatial distribution, Figure 1 presents fire counts in Italy throughout the year 2023. In particular, it shows the counts by region of the

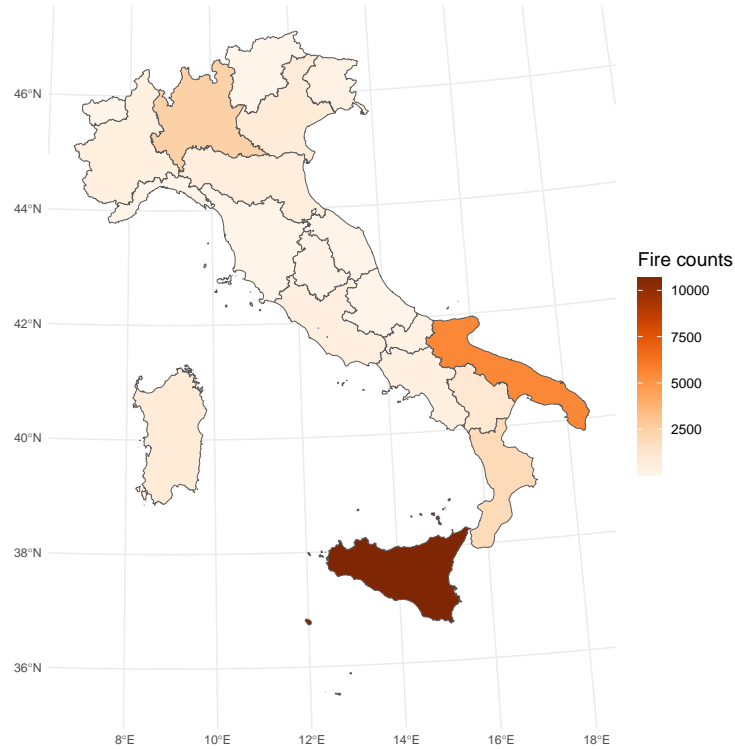


Fig. 1 Choropleth map displaying the counts of the wildfires that occurred in each Italian region during 2023.

26,724 fires that occurred in Italy in 2023. Notably, the graphical representation emphasizes a pronounced concentration of fires in the Sicilian territory, with the second-highest incidence observed in the Southern region of Puglia (*Apulia*). Following this, Figure 2 compares fire counts that occurred in Italy and Sicily in 2023. It is evident that the summer months, from July to October, stand out as critical periods with the highest number of fires. Specifically, July emerges as the most challenging month, recording a total of 8,842 wildfires in Italy, of which 3,814 occurred exclusively in Sicily. Finally, Figure 3 shows the spatial distribution of Sicilian fires in 2023. The inset map (which is reported in the top-left) displays the whole observation window, which includes the mainland of the region and three smaller islands (namely Pantelleria, Lampedusa, and Linosa, respectively), located in the far South and reported

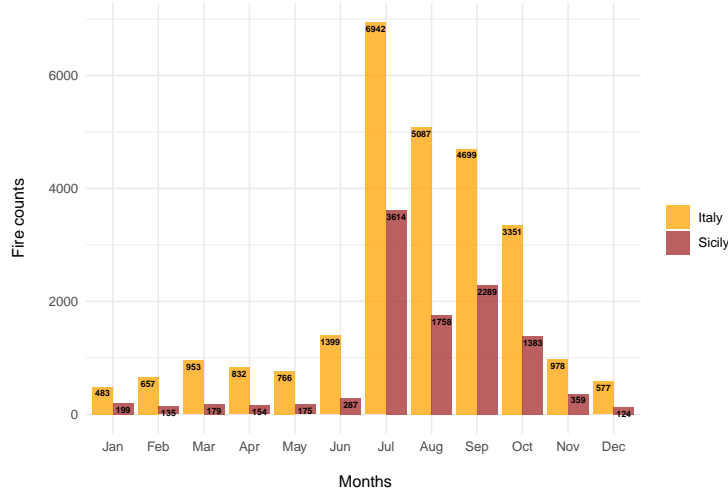


Fig. 2 Barplot comparing the number of fires that occurred in the whole country (yellow bars) and just in the Sicily region (red bars).

in the bottom-left as inset maps. The figure notably indicates clustering behaviour, particularly in the western parts of the mainland.

2.2 Land use

The main focus of our work is the analysis of the fire occurrences depending on the land usage since, as noted later, this type of information can be used as a spatial covariate for our purposes. The land use data come from the CORINE Land Cover (CLC) dataset¹, which is a comprehensive land cover and land-use database created by the European Environment Agency (EEA) to facilitate environmental monitoring and assessment across Europe. It is usually employed to provide insights into the changing landscapes of Europe, aiding in several projects such as environmental management and spatial planning, in addition to wildfire analysis as exemplified in this paper. Combining satellite imagery (obtained from Sentinel-2 and Landsat-8 projects) and ground-based information, CLC classifies land cover into a hierarchical raster system of over 40 classes, including urban areas, forests, water bodies, and agricultural lands. The detailed classification according to CLC comes in Table 1, whereas the product documentation and the nomenclature guidelines can be browsed on the project’s website².

Figure 4 depicts the downloaded data on land usage categorized by level 1 of the CLC Legend after merging the 4th and 5th categories, i.e. wetlands and water bodies (“waterbodies” from now on). In particular, we represent the macro land usage classification, whose categories are:

¹URL: <https://land.copernicus.eu/en/cart-downloads>; Data downloaded during 2023-11

²URL: <https://land.copernicus.eu/content/corine-land-cover-nomenclature-guidelines/html/>. Last access: Feb. 2024.

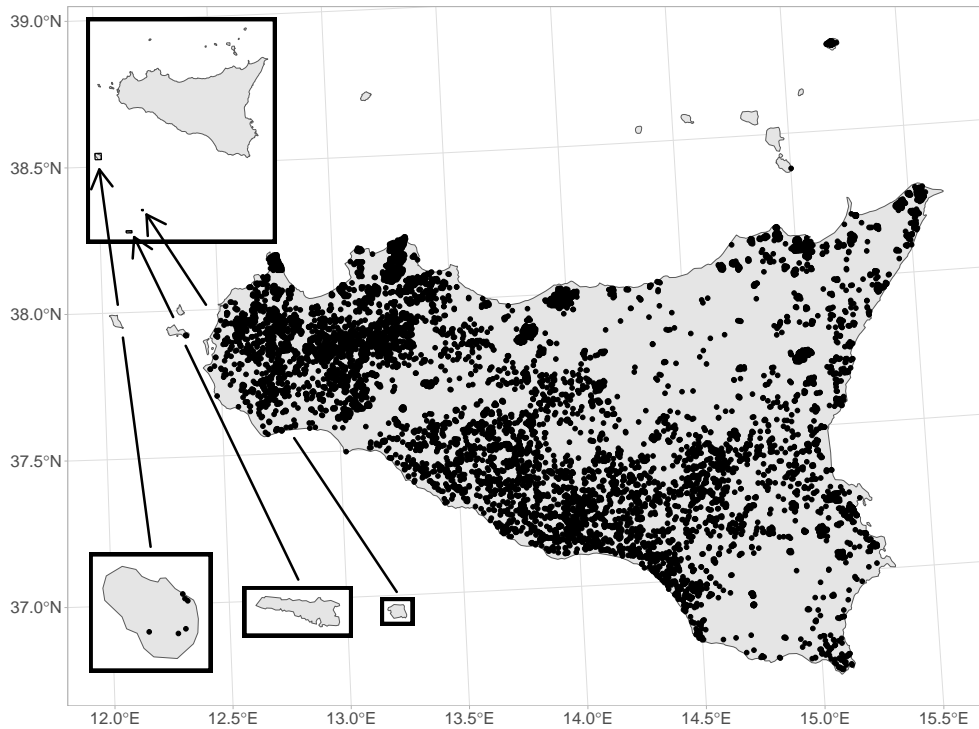


Fig. 3 Spatial distribution of fires recorded in the Sicily region during 2023. The inset map reported in the top-left displays the whole observation window which includes the mainland and three smaller islands (namely Pantelleria, Lampedusa, and Linosa, respectively), located in the far South and reported in the bottom-left as inset maps.

- Artificial surfaces
- Agricultural areas
- Forest and semi-natural areas
- Water bodies

As shown in Table 2, the majority of the Sicilian territory is constituted by agricultural areas (68%, mainly in the southern parts of the region), followed by forests and semi-natural areas (26%, typically located in proximity of some mountain chains in the North and North-East areas). Then, artificial surfaces and water bodies represent the smallest portion (5% and 1%, respectively).

2.3 Environmental covariates

The other covariates considered in this work are now introduced, detailing the sources from where we downloaded the raw data and explaining the pre-processing operations adopted to convert them into an usable format.

Table 1 Land Use Classification according to Corine Land Cover Legend.

Level 1	Level 2	Level 3
Artificial surfaces	Urban fabric Industrial, commercial and transport units Mine, dump and construction sites Artificial, non-agricultural vegetated areas	Continuous urban fabric Discontinuous urban fabric Industrial or commercial units Road and rail networks and associated land Port areas Airports Mineral extraction sites Dump sites Construction sites Green urban areas Sport and leisure facilities
Agricultural areas	Arable Land Permanent crops Heterogeneous agricultural areas	Non-irrigated arable land Permanently irrigated land Vineyards Fruit trees and berry plantations Olive groves Annual crops associated with permanent crops Complex cultivation patterns Land principally occupied by agriculture with significant areas of natural vegetation
Forest and semi-natural areas	Forests Scrub and/or herbaceous vegetation associations Open spaces with little or no vegetation	Broad-leaved forest Coniferous forest Mixed forest Natural grasslands Moors and heathland Sclerophyllous vegetation Transitional woodland-shrub Beaches dunes sands Bare rocks Sparsely vegetated areas Burnt areas
Wetlands	Inland wetlands Marine wetlands	Inland marshes Salt marshes Salines
Water bodies	Inland waters Marine waters	Water courses Water bodies Coastal lagoons Sea and ocean

First, we downloaded the Digital Elevation Model (DEM) data for the Sicily region from the webpage³ of the National Institute of Geophysics and Vulcanology (Tarquini et al., 2023). Starting from the DEM of the whole country, we selected the tiles belonging to the Sicily region and combined them to obtain a unique raster object with 10m resolution that represents the altitude in the area of interest. Then, we used the Horn’s formula (Horn, 1981; Weih Jr and Mattson, 2004) through the GDAL DEM utility command-line tool (GDAL/OGR contributors, 2023) to derive the slope from

³URL: https://tinality.pi.ingv.it/Download_Area1.1.html. Last access: Nov. 2023.

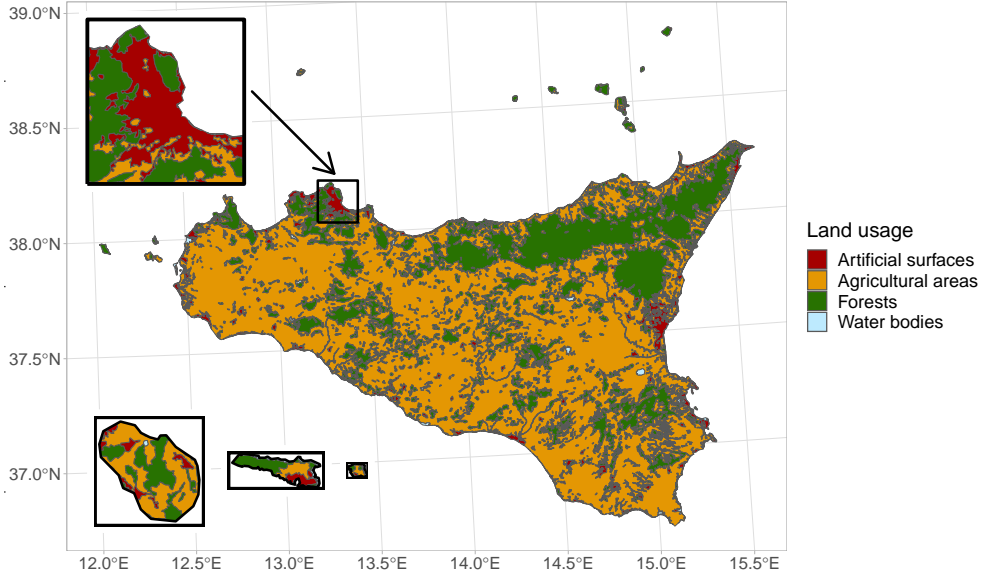


Fig. 4 Land usage in Sicily as reported in the CORINE Land Cover dataset. The inset map included in the top-left zooms around the area of Palermo (which is the capital of the region), whereas the three inset maps displayed in the bottom-left showcase the land usage for Pantelleria, Lampedusa, and Linosa.

Table 2 Area percentage, number of fires, and number of fires over the area percentage of the macro land usage.

	Area perc.	Points	Points perc.
Artificial surfaces	0.050	858	0.081
Agricultural areas	0.683	6529	0.613
Forest and semi-natural areas	0.259	3224	0.303
Water bodies	0.007	45	0.004

the DEM data. More precisely, the Horn's formula says that the slope ϕ can be derived as

$$\phi = \arctan \left(\sqrt{\frac{\partial \text{Alt}}{\partial \text{lon}} + \frac{\partial \text{Alt}}{\partial \text{lat}}} \right) \quad (1)$$

where Alt denotes the altitude dimension and $\partial \text{Alt} / \partial \text{lon}$ and $\partial \text{Alt} / \partial \text{lat}$ represent variations in the East-West and North-South axis, respectively. The two partial derivatives in Equation (1) can be approximated by using finite-order methods such as

$$\frac{\partial \text{Alt}}{\partial \text{lon}} = \frac{(\text{Alt}_1 + 2\text{Alt}_2 + \text{Alt}_3) - (\text{Alt}_7 - 2\text{Alt}_6 + \text{Alt}_5)}{8\Delta \text{lon}} \quad (2)$$

	Alt₁	Alt₈	Alt₇
Latitude	Alt₂	Alt₀	Alt₆
	Alt₃	Alt₄	Alt₅
	Longitude		

Fig. 5 Grid map displaying the relationship between the raster cells used to approximate the variations in the axis directions as used in Equation (2).

where Alt_1, \dots, Alt_7 denote the altitude values in a 3×3 grid surrounding the cell under analysis (i.e. the cell in the middle of the grid), following the scheme detailed in Figure 5 and Δlon represents the spacing between points in the horizontal direction. Similar considerations hold for the estimation of $\partial Alt / \partial lat$ and we refer to [Weih Jr and Mattson \(2004\)](#) and the GDAL DEM webpage⁴ for more details.

The altitude and slope covariates are displayed in the top panel of Figure 6. As we can see, the first map clearly highlights the Etna volcano (located in the eastern part of the region), the mountain chains in the North and North-East areas (Monti Nebrodi), and the Catania valley surrounding the homonymous city. The slope surface is generally flat or almost flat, apart from some regions in the North-East (near Messina).

Finally, Copernicus ERA5 data contains many environmental covariates that were downloaded from <https://cds.climate.copernicus.eu/cdsapp#!/dataset/reanalysis-era5-land?tab=overview>. All of them are obtained in a 38×34 spatial grid with $10\text{km} \times 10\text{km}$ raster cells and hourly resolution for each day of the year. The values are averaged daily over the whole year to match the temporal resolution of fires data. The bottom panel of Figure 6 contains an example of the spatio-temporal resolution of such variables, and the complete description of the available covariates comes as follows.

The $10u$ and $10v$ variables are the eastward and northward components, respectively, of the 10m wind. They represent the horizontal speed of air moving towards the East and North, at a height of ten metres above the surface of the Earth, in metres per second. In particular, the U wind component is parallel to the x -axis (i.e. longitude) while the V wind component is parallel to the y -axis (i.e. latitude). In particular, a positive U wind comes from the West, and a positive V wind comes from the South.

The surface pressure sp is the pressure (force per unit area) of the atmosphere on the surface of land, sea and in-land water. It is a measure of the weight of all the air in

⁴URL: <https://gdal.org/programs/gdaldem.html>

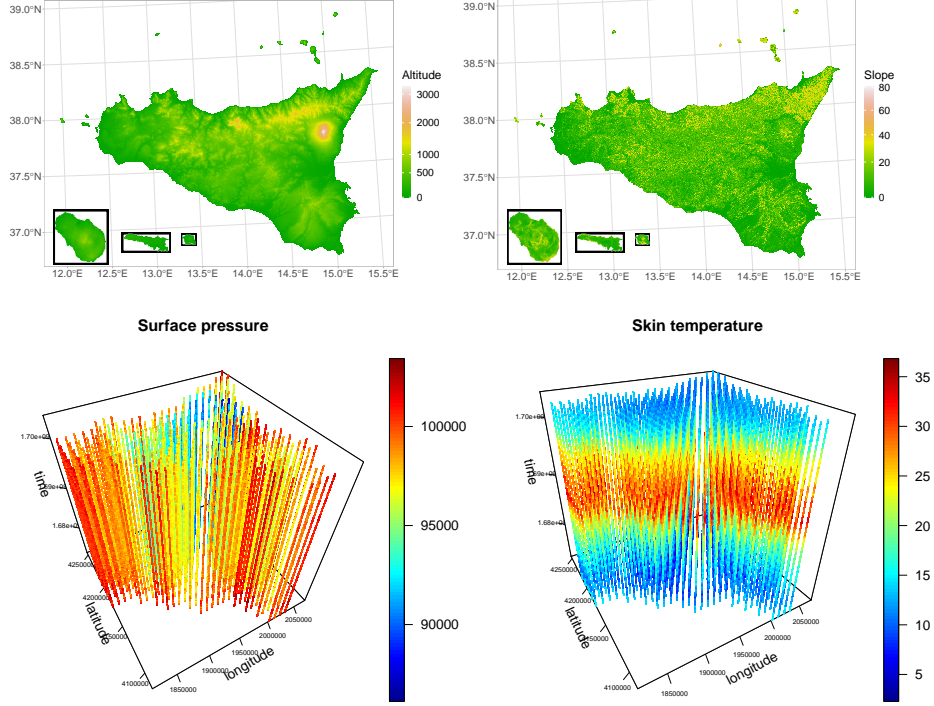


Fig. 6 *Top panels:* Spatial covariates representing the elevation and slope in Sicily: $Z_{elev}(u)$ and $Z_{slope}(u)$; *Bottom panels:* Daily means of the surface pressure and skin temperature in Sicily in 2023.

a column vertically above the area of the Earth’s surface represented at a fixed point. The units of this variable are Pascals (Pa).

The total precipitation τp is the accumulated liquid and frozen water, comprising rain and snow, that falls to the Earth’s surface, not including fog, dew or the precipitation that evaporates in the atmosphere before it lands at the surface of the Earth. This variable is the total amount of water accumulated over a particular time period, which depends on the data extracted. The units of this variable are depth in metres of water equivalent.

The dew point temperature $d2m$ is the temperature to which the air, at 2 metres above the surface of the Earth, would have to be cooled for saturation to occur. The air temperature at 2m above the surface of land, sea or in-land waters is indicated by $\tau 2m$. The skin temperature skt is the temperature of the surface of the Earth, that is, the theoretical temperature that is required to satisfy the surface energy balance. It represents the temperature of the uppermost surface layer, which has no heat capacity and so can respond instantaneously to changes in surface fluxes. All the soil temperatures $st11$, $st12$, $st13$, and $st14$ are the temperature of the soil in the middle of that given

layer. The Advancing global NWP through international collaboration (ECMWF) Integrated Forecasting System (IFS) has a four-layer representation of soil, where the surface is at 0cm. Layer 1: 0 - 7cm; Layer 2: 7 - 28cm; Layer 3: 28 - 100cm; Layer 4: 100 - 289cm. Soil temperature is set at the middle of each layer, and heat transfer is calculated at the interfaces between them. It is assumed that there is no heat transfer out of the bottom of the lowest layer. All the variables representing temperatures have units of kelvin (K), but have been converted to degrees Celsius (C) by subtracting 273.15 in this paper. They are calculated by interpolating between the lowest model level and the Earth's surface, taking account of the atmospheric conditions.

3 Spatio-temporal point processes

We consider a spatio-temporal point process with no multiple points as a random countable subset X of $\mathbb{R}^2 \times \mathbb{R}$, where a point $(u, t) \in X$ corresponds to an event at $u \in \mathbb{R}^2$ occurring at time $t \in \mathbb{R}$. A typical realisation of a spatio-temporal point process X on $\mathbb{R}^2 \times \mathbb{R}$ is a finite set $\{(u_i, t_i)\}_{i=1}^n$ of distinct points within a bounded spatio-temporal region $W \times T \subset \mathbb{R}^2 \times \mathbb{R}$, with area $|W| > 0$ and length $|T| > 0$, where $n \geq 0$ is not fixed in advance. In this context, $N(A \times B)$ denotes the number of points of a set $(A \times B) \cap X$, where $A \subseteq W$ and $B \subseteq T$. As usual (Daley and Vere-Jones, 2007), when $N(W \times T) < \infty$ with probability 1, which holds e.g. if X is defined on a bounded set, we call X a finite spatio-temporal point process.

For a given event (u, t) , the events that are close to (u, t) in both space and time, for each spatial distance r and time lag h , are given by the corresponding spatio-temporal cylindrical neighbourhood of the event (u, t) , which can be expressed by the Cartesian product as

$$b((u, t), r, h) = \{(v, s) : \|u - v\| \leq r, |t - s| \leq h\}, \quad (u, t), (v, s) \in W \times T,$$

where $\|\cdot\|$ denotes the Euclidean distance in \mathbb{R}^2 and $|\cdot|$ is the absolute value. Note that $b((u, t), r, h)$ is a cylinder with centre (u, t) , radius r , and height $2h$.

Product densities $\lambda^{(k)}$, $k \in \mathbb{N}$ and $k \geq 1$, arguably the main tools in the statistical analysis of point processes, may be defined through the so-called Campbell Theorem (see Daley and Vere-Jones (2007)), that constitutes an essential result in spatio-temporal point process theory. It states that, given a spatio-temporal point process X , for any non-negative function f on $(\mathbb{R}^2 \times \mathbb{R})^k$

$$\mathbb{E} \left[\sum_{\substack{\neq \\ \zeta_1, \dots, \zeta_k \in X}} f(\zeta_1, \dots, \zeta_k) \right] = \int_{\mathbb{R}^2 \times \mathbb{R}} \cdots \int_{\mathbb{R}^2 \times \mathbb{R}} f(\zeta_1, \dots, \zeta_k) \lambda^{(k)}(\zeta_1, \dots, \zeta_k) \prod_{i=1}^k d\zeta_i,$$

where \neq indicates that the sum is over distinct values. In particular, for $k = 1$ these functions are called the *intensity function* λ . Broadly speaking, the intensity function describes the rate at which the events occur in the given spatio-temporal region, representing the point process analogues of the mean function of a real-valued process.

Then, the first-order intensity function is formally defined as

$$\lambda(u, t) = \lim_{|du \times dt| \rightarrow 0} \frac{\mathbb{E}[N(du \times dt)]}{|du \times dt|},$$

where $du \times dt$ defines a small region around the point (u, t) and $|du \times dt|$ is its volume.

3.1 Spatio-temporal Poisson point processes with separable intensity

The description of the observed point pattern intensity is a crucial issue when dealing with spatio-temporal point pattern data, and specifying a statistical model is a very effective way compared to analyzing data by calculating summary statistics. Formulating and adapting a statistical model to the data allows taking into account effects that otherwise could introduce distortion in the analysis (Baddeley et al., 2015).

When dealing with intensity estimation for spatio-temporal point processes, it is quite common to assume that the intensity function $\lambda(u, t)$ is separable (Diggle, 2013; Gabriel and Diggle, 2009). Under this assumption, the intensity function is given by the product

$$\lambda(u, t) = \lambda(u)\lambda(t) \quad (3)$$

where $\lambda(u)$ and $\lambda(t)$ are non-negative functions on W and T , respectively. Suitable estimates of $\lambda(u)$ and $\lambda(t)$ in Equation (3) depend on the characteristics of each application. This formulation can include a combination of a parametric spatial point pattern model, potentially depending on the spatial coordinates and/or spatial covariates, and a parametric log-linear model for the temporal component. Also, non-parametric kernel estimate forms are legit. The spatio-temporal intensity is therefore obtained by multiplying the purely spatial and purely temporal intensities, previously fitted separately. The resulting intensity is normalised, to make the estimator unbiased, making the expected number of points

$$\mathbb{E} \left[\int_{W \times T} \hat{\lambda}(u, t) d_2(u, t) \right] = \int_{W \times T} \lambda(u, t) d_2(u, t) = n,$$

and the final intensity function is obtained as

$$\hat{\lambda}(u, t) = \frac{\hat{\lambda}(u)\hat{\lambda}(t)}{\int_{W \times T} \hat{\lambda}(u, t) d_2(u, t)}.$$

3.2 Spatial component

A general spatial log-linear Poisson model (Cox, 1972), generalizes both homogeneous and inhomogeneous models, such that:

$$\lambda(u) = \exp(\boldsymbol{\theta}^\top \mathbf{Z}(u)), \quad (4)$$

where $u \in W$, and $\mathbf{Z}(u) = \{Z_1(u), \dots, Z_p(u)\}$ are known covariate functions, $\boldsymbol{\theta}^\top = (\theta_1, \dots, \theta_p)$ are unknown parameters, and therefore $\boldsymbol{\theta}^\top \mathbf{Z}(u) = (\theta_1 Z_1(u) + \dots + \theta_p Z_p(u))$. These models have an especially convenient structure, since the log intensity is a linear function of the parameters and covariates can be quite general functions, making them a very wide class of models. The estimation of the point process parameters is carried out through the maximization of the log-likelihood, defined by:

$$\log L(\boldsymbol{\theta}) = \sum_i \log \lambda(x_i; \boldsymbol{\theta}) - \int_W \lambda(u; \boldsymbol{\theta}) du \quad (5)$$

where the sum is over all points x_i in the point process \mathbf{x} (Daley and Vere-Jones, 2007). For estimation purposes, we use a finite quadrature approximation of the log-likelihood, following Berman and Turner (1992), that is, starting from the observed points u_1, \dots, u_n , generate m additional *dummy points* u_{n+1}, \dots, u_{n+m} to form a set of $n+m$ quadrature points (where $m > n$). Then, integral in (5) is approximated by the Riemann sum

$$\int_W \lambda(u; \boldsymbol{\theta}) du \approx \sum_{k=1}^{n+m} a_k \lambda(u_k; \boldsymbol{\theta})$$

where a_1, \dots, a_m are quadrature weights and $\sum_{k=1}^{n+m} a_k = l(W)$, with $l(\cdot)$ the Lebesgue measure. In order to distinguish between dummy points and observed points, we introduce the indicator e_k , which assumes values equal to 1 if the related point is a data point, zero otherwise. Then, writing $y_k = e_k/a_k$, the log-likelihood (5) of the template model can be approximated by $\log L(\boldsymbol{\theta}) \approx \sum_j a_j (y_j \log \lambda(u_j; \boldsymbol{\theta}) - \lambda(u_j; \boldsymbol{\theta})) + \sum_k a_k$. Apart from the constant $\sum_k a_k$, this expression is formally equivalent to the weighted log-likelihood of a Poisson regression model with responses y_k and means $\lambda(u_k, t_k; \boldsymbol{\theta}) = \exp(\boldsymbol{\theta}^\top \mathbf{Z}(u_k, t_k))$. This means that the model can be maximised using standard GLM software, but also that covariate values must be known in every data and dummy point location. Indeed, the spatial covariates are referred to as those variables with observable values, at least in principle, at each spatial location in the spatial window, and for the inferential purposes given above, their values must be known at each point of the data point pattern and at least at some other locations.

3.2.1 Diagnostics

For an inhomogeneous Poisson process model, with fitted intensity $\hat{\lambda}(u)$, the predicted number of points falling in any region W is $\int_W \hat{\lambda}(u) du$. Hence, the residual in each region $W \subset \mathbb{R}^2$ is the ‘observed minus predicted’ number of points falling in W (Alm, 1998), that is $R(W) = n(\mathbf{x} \cap W) - \int_W \hat{\lambda}(u) du$, where \mathbf{x} is the observed point pattern, $n(\mathbf{x} \cap W)$ the number of points of \mathbf{x} in the region W , and $\hat{\lambda}(u)$ is the intensity of the fitted model. A simple residual visualization can be obtained by smoothing them. The ‘smoothed residual fields’ are defined as

$$s(u) = \tilde{\lambda}(u) - \lambda^\dagger(u) \quad (6)$$

where $\tilde{\lambda}(u) = e(u) \sum_{i=1}^{n(\mathbf{x})} \kappa(u - \mathbf{x}_i)$ is the non-parametric, kernel estimate of the fitted intensity $\hat{\lambda}(u)$, while $\lambda^\dagger(u)$ is a correspondingly-smoothed version of the (typically parametric) estimate of the intensity of the fitted model, $\lambda^\dagger(u) = e(u) \int_W \kappa(u - v) \hat{\lambda}(v) dv$. Here, κ is the smoothing kernel and $e(u)$ is the edge correction. The smoothing bandwidth for the kernel estimation of the raw residuals is selected by cross-validation, as the value that minimises the Mean Squared Error criterion defined by [Diggle \(1985\)](#) by the method of [Berman and Diggle \(1989\)](#).

The differences in Equation (6) should be approximately zero when the fitted model is close to the real one. Therefore, the best model is the one with the lowest values of the smoothed raw residuals. Their graphical representation gives further insights on which spatial regions the model could not be a good fit.

3.3 Temporal component

Temporal count data analysis often involves modelling the occurrence of events over time, and a suitable statistical approach is essential to capture the temporal dynamics adequately. In this context, the Poisson regression model, which belongs to the class of Generalized Linear Models (GLMs), provides a robust framework for analyzing count data exhibiting temporal variation.

Consider a set of covariates $\mathbf{Z}(t) = \{Z_1(t), \dots, Z_q(t)\}$ influencing the event rate. The temporal count Poisson model is then formulated as follows:

$$\lambda(t) = \exp(\boldsymbol{\beta}^T \mathbf{Z}(t)).$$

Here, $t \in T$ and $\boldsymbol{\beta} = \{\beta_0, \beta_1, \dots, \beta_q\}$ are the model parameters associated with the temporal covariates.

The model parameters are estimated through the maximum likelihood estimation (MLE) method within the GLM framework ([McCullagh and Nelder, 1989](#)).

After fitting the model, assessing its performance involves standard GLM techniques such as residual analysis, goodness-of-fit tests, and validation on independent datasets. Interpretation of the model parameters provides insights into the impact of covariates and temporal components on the event rate over time.

A generalized additive model (GAM) is a GLM in which the linear predictor is given by a sum of smooth functions of the covariates plus a conventional parametric component. In such a case, we may write $\lambda(t) = \exp(f(\mathbf{Z}(t)))$ where $f(\cdot)$ is a smooth function of the covariate \mathbf{Z} . The smooth terms can be functions of any number of covariates, and the control over the smoothness of the functions is solved by using the Generalized Cross Validation (GCV) criterion ([Wood, 2017](#)).

4 Results

In this section, we present the results obtained fitting the separable spatio-temporal intensity function presented in Section 3 to the data introduced in Section 2. Specifically, in Section 4.1, a spatial log-linear Poisson point process model is applied to investigate the influence of land use types on the purely spatial fire distribution, accounting for other environmental covariates. In Section 4.2, a Poisson Generalized

	Estimate	Std. Error	z value	p value
Intercept	-15.129	0.040	-376.580	$< 1 \times 10^{-3}$
Agricultural areas	-0.286	0.040	-7.179	$< 1 \times 10^{-3}$
Forest and semi-natural areas	-0.540	0.046	-11.727	$< 1 \times 10^{-3}$
Wetlands and water bodies	-0.595	0.154	-3.870	$< 1 \times 10^{-3}$
Elevation	1.675	0.040	42.320	$< 1 \times 10^{-3}$
Slope	0.006	0.001	4.768	$< 1 \times 10^{-3}$

Table 3 Estimated coefficients of the fitted spatial model in Equation (7).

Additive Model is fitted to the temporal fire occurrences, depending on both non-parametric components of the temporal coordinates and parametric formulation of environmental covariates.

4.1 Spatial intensity

Starting from the maximal model and proceeding with a backwards procedure based on the comparison of the AIC values and the sequential performance of tests for the significance of the model parameters, the chosen spatial model has a linear predictor that includes a non-parametric term for the spatial coordinates and parametric expression for the spatial covariates, as follows

$$\lambda(u) = \exp(f(u) + \theta_1 Z_{land_use}(u) + \theta_2 Z_{elev}(u) + \theta_3 Z_{slope}(u)). \quad (7)$$

Here, $f(\cdot)$ is a nonparametric function for $u \in W$, estimated through thin plate regression splines (Wood, 2003) with 30 knots.

Table 3 presents the results from the fitted spatial Poisson model that investigates the influence of various factors on fire occurrence. In addition to the intercept, the first three rows correspond to the categories of the *land use* variable, with *Artificial surfaces* serving as the baseline. Also note that the elevation has been converted from meters to kilometres, to obtain estimated coefficients on the same magnitude as the other ones.

Considering different land usages, agricultural areas show a significant negative estimated parameter, signifying a considerable decrease in the fire occurrence intensity moving from artificial surfaces to agricultural ones. Forest and semi-natural areas also show a negative effect, although with a higher magnitude compared to agricultural areas. Then, wetlands and water bodies also display a significant negative parameter, albeit with a wider confidence interval, indicating greater uncertainty. This is likely due to the sparsity of the area covered in Sicily by this type of land. Lastly, both elevation and slope exhibit a significant effect, with their increase being associated with higher intensity. Note that an attempt has been made to assess the significance of the ERA5 spatio-temporal covariates, averaged over time. However, these purely spatial covariates did not influence the overall spatial occurrence of fires and therefore were not included in the chosen model. This is likely due to the very coarse grid of the obtained spatial covariates if compared to those representing elevation and slope (top panels of Figure 6).

Among the perks of fitting a semi-parametric model as the one in Equation (7) there is the smoothed prediction map that can be obtained, as shown in the left panel of Figure 7. The smoothed raw residuals in the right panel of Figure 7, computed as detailed in Section 3.2.1, indicate a good model fitting, exhibiting almost all residuals approaching zero.

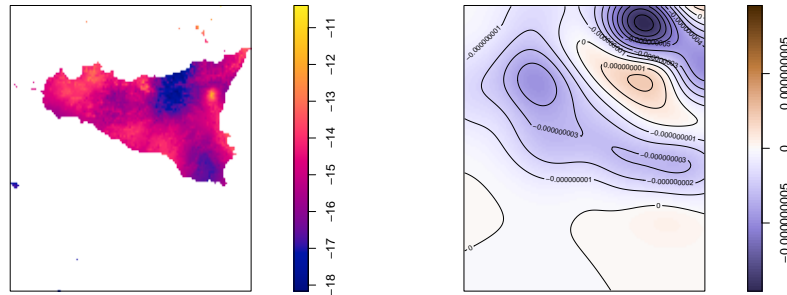


Fig. 7 *Left panel:* Intensity predicted according to the fitted spatial model in Equation (7); *Right panel:* Smoothed raw residuals of the fitted model.

4.2 Temporal intensity

Following the same backward procedure adopted for the spatial component, the chosen temporal model comes with a linear predictor that includes a non-parametric term for temporal coordinates and parametric expression for the temporal covariates, as follows:

$$\lambda(t) = \exp(f(t) + \beta_1 Z_{v10}(t) + \beta_2 Z_{stl2}(t) + \beta_3 Z_{sp}(t) + \beta_4 Z_{tp}(t)), \quad (8)$$

with $f(\cdot)$ a nonparametric function for $t \in T$, estimated through penalized regression basis splines (Wood, 2017) with 50 knots.

	Estimate	Std. Error	z value	p value
Intercept	77.314	5.471	14.133	$< 1 \times 10^{-3}$
Wind speed from South	0.232	0.008	30.426	$< 1 \times 10^{-3}$
Temperature	0.440	0.024	18.672	$< 1 \times 10^{-3}$
Surface pressure	-0.001	0.000	-16.251	$< 1 \times 10^{-3}$
Total precipitation	-14.848	2.266	-6.553	$< 1 \times 10^{-3}$

Table 4 Estimated coefficients of the fitted temporal model in Equation (8).

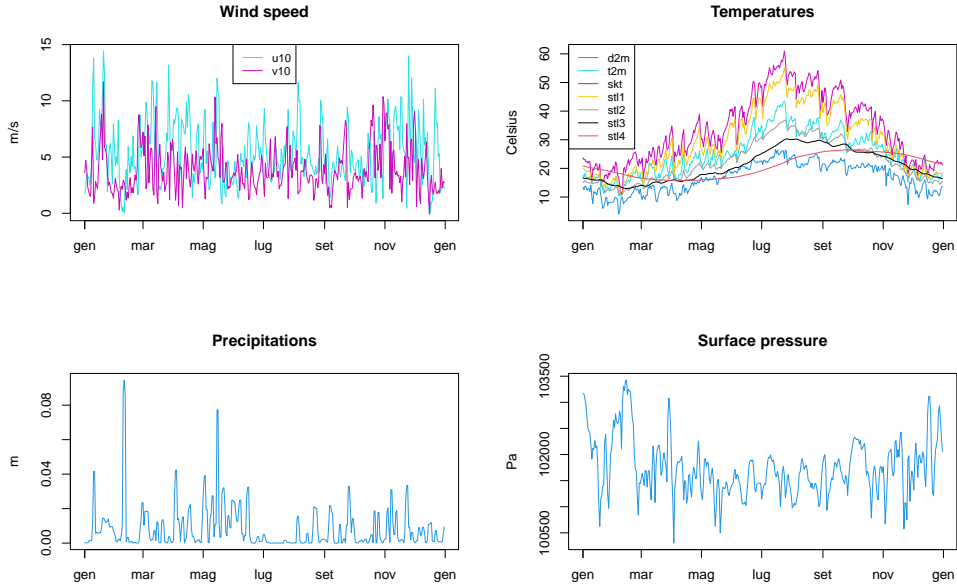


Fig. 8 Daily maxima of the wind components, temperatures, precipitation and surface pressure

In order to fit this model, the ERA5 environmental spatio-temporal covariates have been averaged with respect to the spatial components, making them purely temporal covariates. Moreover, the results of the models fitted with the daily means of such covariates have been compared to those containing the daily maxima, and the latter yielded better fitting. The resulting temporal covariates are shown in Figure 8. As evident, the temperatures appear highly correlated among themselves and with the time of the year. In detail, the deeper the surface layers of detection, the smoother the temperature variability. Figure 9 further illustrates such high correlations, especially among temperature variables. Table 4 outlines the outcomes of the fitted model, whose detailed breakdown follows.

Wind speed demonstrates a notable positive influence, implying that higher wind speeds from the South correlate with increased fire counts, highlighting the role of the Scirocco wind in wildfire dynamics. This Mediterranean wind that comes from the Sahara brings heat and dust from African coastal regions. Temperature shows a significant positive relationship with fire counts. Pressure exhibits a negative estimated parameter, suggesting that higher atmospheric pressure is associated with lower fire counts, hinting at its potential suppressive effect. Precipitation reveals a substantial negative effect, indicating fewer fire counts with higher daily precipitation, highlighting its mitigating effect.

The significant smooth terms suggest that time plays a crucial role in the observed residual variability of fire incidents, not taken into account by the environmental covariates.

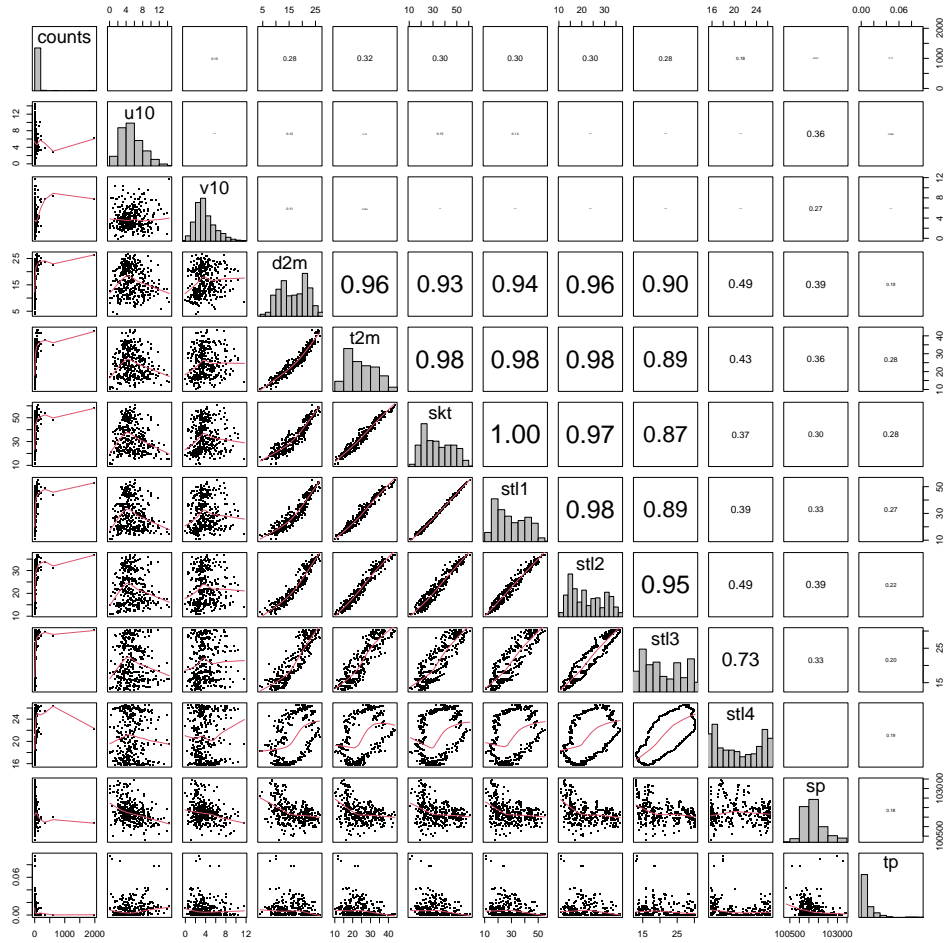


Fig. 9 Correlations among the temporal covariates and the daily fire counts over 2023. On the main diagonal, the univariate distributions of the variables. On the lower panels, the scatterplots of each pair of variables with a smoothing function overlapped in red. On the upper panels, the correlations among the variables.

An adjusted R-squared of 0.738 and an 83.9% of deviance explained indicates that the model explains substantial variability in fire counts. Figure 10 shows the intensity predicted according to the fitted model in Equation (8), demonstrating a good ability to capture the temporal variability of fire counts.

5 Discussion and conclusions

The proposed analysis of the spatial and temporal distribution of fire occurrences in Sicily during 2023 has provided insights into the factors influencing these events, with

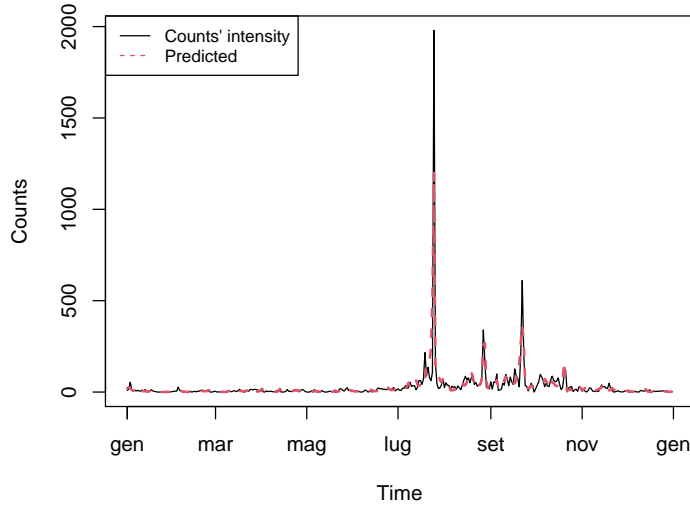


Fig. 10 Temporal intensity predicted according to the fitted temporal model in Equation (8) (red dashed line) and the observed fire counts (solid line).

a particular emphasis on the role of land usage. Our findings highlight the significance of human activities in contributing to the prevalence of fires. The identification of artificial surfaces as a key contributor to the increased probability of fire occurrence highlights the urgent need for targeted intervention and policy measures. The implications of this research are particularly pertinent, considering the well-established fact that the majority of fires in Sicily are human-induced (Ferrara et al., 2019). These results have broader implications for regional planning, resource allocation, and the development of proactive measures to manage fire risks effectively. Recognizing the human-centric nature of fire occurrences prompts us to advocate for sustainable land-use practices and the implementation of policies aimed at minimizing the risk of fires in areas characterized by artificial surfaces. Our analysis extends beyond land usage, incorporating environmental covariates that significantly influence the occurrence of fires in Sicily during 2023. Our findings reveal a significant role of these environmental factors over the temporal event occurrences. Particularly, wind speed from the South and temperature emerge as crucial variables, emphasising the importance of climatic conditions in amplifying fire risks. Conversely, our study identifies surface pressure and total precipitation as environmental covariates that negatively influence fire occurrences as mitigating factors. Additionally, our research highlights the significance of terrain characteristics in explaining the spatial distribution of fire points. In particular, both elevation and slope exhibit a positive effect on the occurrence of fires, indicating that areas with higher elevations and steeper slopes are more susceptible.

Note that other FIRMS variables could have been used in this paper. These are the brightness temperature in Kelvin, the along scan and track pixel sizes, the type

of satellite, a confidence value attached to each individual hotspot/fire pixel, the collection/version source, the Fire Radiative Power, in megawatts, and whether the fire occurred during daytime or nighttime. The main reason for not using this type of covariates is that, in point process theory, they are referred to as “marks” of the observed point pattern (Daley and Vere-Jones, 2007). While the spatial covariates are referred to as those variables with observable values, at least in principle, at each spatial location in the spatio-temporal window, marks are characteristics of the events, which are attached to the points of the observed patterns and can be studied to explore their eventual aid in describing the phenomenon under study. Formally, however, their inclusion in a regression-type model is quite different if compared to the will to include the so-called spatial or spatio-temporal covariates. Indeed, the latter covariates are characteristics of the spatial or spatio-temporal region, and their inclusion in a regression-type point process model is more straightforward, not needing any particular assumption on, for instance, their distribution. Moreover, the literature on the so-called marked point process methodologies is rather specific to particular physical phenomena, like the seismic ones with the ETAS models (Ogata, 1988), and quite limited for the cases in the presence of multiple marks. This is why we decided not to include marks in our analysis, even though we believe it represents a very interesting topic, both from the methodological and the applied points of view.

Moving to other possible future research paths, a major topic that could be addressed is the definition and application of tailored diagnostic procedures to assess the need for more complex models in case of residual clustering behaviour of points not taken into account by the already considered factors. Indeed, the employment of most known diagnostic tools based on second-order summary statistics (Adelfio and Schoenberg, 2009; Adelfio et al., 2020), both global and local, becomes computationally hard as the number of points increases. In a preliminary way, it is worth noticing that one could first run a test for first-order separability prior to fitting the model. In particular, Schoenberg (2004), Díaz-Avalos et al. (2013), and Fuentes-Santos et al. (2018) show that the intensity of forest fire occurrences varies in space and time in a nonseparable way. We, however, believe that our proposed model overcomes computational burden issues, typical of more complex non-separable spatio-temporal models.

Moreover, the inclusion and test of spatially (or spatio-temporally) varying covariates in intensity function has been of particular interest in Díaz-Avalos et al. (2014), Borrajo et al. (2017, 2020b,a) and Myllymäki et al. (2021). Following these, future work includes the assessment of separability assumption, as well as exploring more complex models, like the log-Gaussian Cox processes, multitype Poisson models, and local ones (D’Angelo et al., 2023).

Fundings

The research work of Nicoletta D’Angelo and Giada Adelfio was supported by:

- Targeted Research Funds 2024 (FFR 2024) of the University of Palermo (Italy);
- Mobilità e Formazione Internazionali - Miur INT project “Sviluppo di metodologie per processi di punto spazio-temporali marcati funzionali per la previsione probabilistica dei terremoti”;

- European Union - NextGenerationEU, in the framework of the GRINS - Growing Resilient, INclusive and Sustainable project (GRINS PE00000018 – CUP C93C22005270001).

Andrea Gilardi acknowledges the support by MUR, grant Dipartimento di Eccellenza 2023-2027. His research work is funded by the European Union - NextGenerationEU, in the framework of the GRINS - Growing Resilient, INclusive and Sustainable project (GRINS PE00000018 – CUP D43C22003110001).

The research work of Alessandro Albano has been supported by the European Union - NextGenerationEU - National Sustainable Mobility Center CN00000023, Italian Ministry of University and Research Decree n. 1033— 17/06/2022, Spoke 2, CUP B73C2200076000 and Targeted Research Funds 2024 (FFR 2024) of the University of Palermo (Italy).

The views and opinions expressed are solely those of the authors and do not necessarily reflect those of the European Union, nor can the European Union be held responsible for them.

References

- Adelfio, G. and Schoenberg, F. P. (2009). Point process diagnostics based on weighted second-order statistics and their asymptotic properties. *Annals of the Institute of Statistical Mathematics*, 61(4):929–948.
- Adelfio, G., Siino, M., Mateu, J., and Rodríguez-Cortés, F. J. (2020). Some properties of local weighted second-order statistics for spatio-temporal point processes. *Stochastic Environmental Research and Risk Assessment*, 34(1):149–168.
- Aldersley, A., Murray, S. J., and Cornell, S. E. (2011). Global and regional analysis of climate and human drivers of wildfire. *Science of the Total Environment*, 409(18):3472–3481.
- Alm, S. E. (1998). Approximation and simulation of the distributions of scan statistics for poisson processes in higher dimensions. *Extremes*, 1(1):111–126.
- Baddeley, A., Rubak, E., and Turner, R. (2015). *Spatial point patterns: methodology and applications with R*. Chapman and Hall/CRC.
- Berman, M. and Diggle, P. (1989). Estimating weighted integrals of the second-order intensity of a spatial point process. *Journal of the Royal Statistical Society: Series B (Methodological)*, 51(1):81–92.
- Berman, M. and Turner, T. R. (1992). Approximating point process likelihoods with glim. *Journal of the Royal Statistical Society: Series C (Applied Statistics)*, 41(1):31–38.
- Borrajó, M., González-Manteiga, W., and Martínez-Miranda, M. (2017). Testing first-order intensity model in non-homogeneous poisson point processes with covariates. *arXiv preprint arXiv:1709.07716*.
- Borrajó, M., González-Manteiga, W., and Martínez-Miranda, M. (2020a). Testing for significant differences between two spatial patterns using covariates. *Spatial Statistics*, 40:100379.
- Borrajó, M. I., González-Manteiga, W., and Martínez-Miranda, M. (2020b). Bootstrapping kernel intensity estimation for inhomogeneous point processes with spatial

- covariates. *Computational Statistics & Data Analysis*, 144:106875.
- Butsic, V., Kelly, M., and Moritz, M. A. (2015). Land use and wildfire: A review of local interactions and teleconnections. *Land*, 4(1):140–156.
- Cox, D. (1972). The statistical analysis of dependencies in point processes. *Stochastic Point Processes*. Wiley: New York, pages 55–66.
- Daley, D. J. and Vere-Jones, D. (2007). *An Introduction to the Theory of Point Processes*. Volume II: General Theory and Structure. Springer-Verlag, New York, second edition.
- D’Angelo, N. and Adelfio, G. (2023). *stopp: Spatio-Temporal Point Pattern Methods, Model Fitting, Diagnostics, Simulation, Local Tests*. R package version 0.1.0.
- D’Angelo, N., Adelfio, G., and Mateu, J. (2023). Locally weighted minimum contrast estimation for spatio-temporal log-gaussian cox processes. *Computational Statistics & Data Analysis*, 180:107679.
- Díaz-Avalos, C., Juan, P., and Mateu, J. (2013). Similarity measures of conditional intensity functions to test separability in multidimensional point processes. *Stochastic Environmental Research and Risk Assessment*, 27:1193–1205.
- Díaz-Avalos, C., Juan, P., and Mateu, J. (2014). Significance tests for covariate-dependent trends in inhomogeneous spatio-temporal point processes. *Stochastic environmental research and risk assessment*, 28:593–609.
- Diggle, P. (1985). A kernel method for smoothing point process data. *Journal of the Royal Statistical Society: Series C (Applied Statistics)*, 34(2):138–147.
- Diggle, P. J. (2013). *Statistical analysis of spatial and spatio-temporal point patterns*. Chapman and Hall/CRC.
- Ferrara, C., Salvati, L., Corona, P., Romano, R., and Marchi, M. (2019). The background context matters: Local-scale socioeconomic conditions and the spatial distribution of wildfires in italy. *Science of the Total Environment*, 654:43–52.
- Fuentes-Santos, I., González-Manteiga, W., and Mateu, J. (2018). A first-order, ratio-based nonparametric separability test for spatiotemporal point processes. *Environmetrics*, 29(1):e2482.
- Gabriel, E. and Diggle, P. J. (2009). Second-order analysis of inhomogeneous spatio-temporal point process data. *Statistica Neerlandica*, 63(1):43–51.
- Ganteaume, A., Camia, A., Jappiot, M., San-Miguel-Ayanz, J., Long-Fournel, M., and Lampin, C. (2013). A review of the main driving factors of forest fire ignition over europe. *Environmental management*, 51:651–662.
- GDAL/OGR contributors (2023). *GDAL/OGR Geospatial Data Abstraction software Library*. Open Source Geospatial Foundation.
- Hantson, S., Pueyo, S., and Chuvieco, E. (2015). Global fire size distribution is driven by human impact and climate. *Global Ecology and Biogeography*, 24(1):77–86.
- Horn, B. K. (1981). Hill shading and the reflectance map. *Proceedings of the IEEE*, 69(1):14–47.
- McCullagh, P. and Nelder, J. A. (1989). *Generalised Linear Models*. Chapman and Hall, 2nd edition.
- Myllymäki, M., Kuronen, M., and Mrkvicka, T. (2021). Testing global and local dependence of point patterns on covariates in parametric models. *Spatial Statistics*, 42:100436.

- Ogata, Y. (1988). Statistical models for earthquake occurrences and residual analysis for point processes. *Journal of the American Statistical Association*, 83(401):9–27.
- Pebesma, E. (2018). Simple Features for R: Standardized Support for Spatial Vector Data. *The R Journal*, 10(1):439–446.
- Pebesma, E. and Bivand, R. (2023). *Spatial Data Science: With applications in R*. Chapman and Hall/CRC, London.
- R Core Team (2024). *R: A Language and Environment for Statistical Computing*. R Foundation for Statistical Computing, Vienna, Austria.
- Ricotta, C., Bajocco, S., Guglietta, D., and Conedera, M. (2018). Assessing the influence of roads on fire ignition: does land cover matter? *Fire*, 1(2):24.
- Ricotta, C. and Di Vito, S. (2014). Modeling the landscape drivers of fire recurrence in sardinia (italy). *Environmental management*, 53(6):1077–1084.
- Rodrigues, M. and De la Riva, J. (2014). An insight into machine-learning algorithms to model human-caused wildfire occurrence. *Environmental Modelling & Software*, 57:192–201.
- Schoenberg, F. P. (2004). Testing separability in spatial-temporal marked point processes. *Biometrics*, pages 471–481.
- Tarquini, S., Isola, I., Favalli, M., Battistini, A., and Dotta, G. (2023). *TINITALY, a digital elevation model of Italy with a 10 meters cell size*, 1.1 edition. Istituto Nazionale di Geofisica e Vulcanologia (INGV). <https://doi.org/10.13127/tinitaly/1.1>.
- Weih Jr, R. C. and Mattson, T. L. (2004). Modeling slope in a geographic information system. *Journal of the Arkansas Academy of Science*, 58(1):100–108.
- Wood, S. N. (2003). Thin plate regression splines. *Journal of the Royal Statistical Society Series B: Statistical Methodology*, 65(1):95–114.
- Wood, S. N. (2017). *Generalized additive models: an introduction with R*. CRC press.